International Journal of Nanomedicine

Dovepress
Taylor & Francis Group

Open Access Full Text Article

ORIGINAL RESEARCH

Polydopamine Nanoparticle-Integrated Smart *Bletilla striata* Polysaccharide Hydrogel: Photothermal-Triggered CO_2 Release for Diabetic Wound Microenvironment Modulation

Xiao Wang[1], Zihao Ma[1], Yujie He[1], Ying Sun[1], Qian Peng[1], Ming Zhao[2], Xiaojing Huang[3], Lei Lei[3], Huan Gu[1], Kaijun Gou[1], Rui Zeng[1]

[1]College of Pharmacy and Food, Southwest Minzu University, Chengdu & Key Laboratory of Research and Application of Ethnic Medicine Processing and Preparation on the Qinghai Tibet Plateau, Chengdu, 610225, People's Republic of China; [2]Sichuan Sports College, Chengdu, 610043, People's Republic of China; [3]Chengdu Institute for Drug Control & NMPA Key Laboratory for Quality Monitoring and Evaluation of Traditional Chinese Medicine (Chinese Materia Medica), Chengdu, 610000, People's Republic of China

Correspondence: Rui Zeng, College of Pharmacy and Food, Southwest Minzu University, Chengdu & Key Laboratory of Research and Application of Ethnic Medicine Processing and Preparation on the Qinghai Tibet Plateau, Chengdu, 610225, People's Republic of China, Email rzeng@swun.edu.cn

Purpose: Bacterial infection, oxidative stress, vascular damage, and nutrient deficiencies significantly hinder the repair of diabetic skin wounds. Conventional wound dressings offer limited protection and fail to effectively promote the healing of diabetic wounds. To address these challenges, we developed a photothermal-responsive *Bletilla striata* polysaccharide hydrogel capable of releasing carbon dioxide (CO_2@PDA Hydrogel).

Methods: This hydrogel utilizes carboxymethylated *Bletilla striata* polysaccharide as the primary matrix, cross-linked through metal coordination bonds, and incorporates bicarbonate-containing polydopamine nanoparticles (CO_2@PDA NPs) with photothermal conversion properties to generate CO_2. The structure and morphology of CO_2@PDA NPs were characterized by DLS, SEM, FTIR, and XRD, and the hydrogel properties of CO_2@PDA Hydrogel were characterized by SEM, rheological properties, and FTIR. The photothermal properties of the CO_2@PDA Hydrogel were studied by measuring the temperature change and CO_2 release after irradiation with an NIR laser (808nm). The improvement effect of CO_2@PDA Hydrogel on the diabetes wound microenvironment was comprehensively evaluated by promoting L929 cell proliferation, inhibiting bacterial growth (*Staphylococcus aureus* and *Escherichia coli*), and treating diabetes wound infection in rat models.

Results: Under 808 nm near-infrared laser irradiation, the embedded CO_2@PDA NPs convert light into heat, triggering the decomposition of HCO_3^- and releasing a substantial amount of CO_2 locally at the diabetic wound site. The released CO_2 responds to the Bohr effect, alleviating hypoxia and promoting angiogenesis. Simultaneously, the *Bletilla striata* polysaccharide in the hydrogel exerts antioxidant and anti-inflammatory effects, while the cross-linking agent Fe^{3+} and the photothermal properties of CO_2@PDA NPs provide robust antibacterial activity.

Conclusion: The self-assembled cross-linked carboxymethyl *Bletilla striata* polysaccharide Hydrogel with CO_2@PDA NPs prepared in this study has a good photothermal conversion effect. It improves the microenvironment of diabetes wounds by improving hypoxia, antibacterial, antioxidant, and other effects, providing a good multi-functional alternative material for the treatment of refractory diabetes wounds.

Keywords: multi-functional photothermal hydrogel, polydopamine nanoparticles, improving hypoxia, antibacterial activity, antioxidant effect

Introduction

Difficult wound healing is a common complication of diabetic patients, known as diabetic wounds, which is the main reason that diabetic patients have to amputate. The slow wound healing of patients with diabetic wounds caused by

Received: 27 March 2025
Accepted: 7 June 2025
Published: 8 July 2025

Graphical Abstract

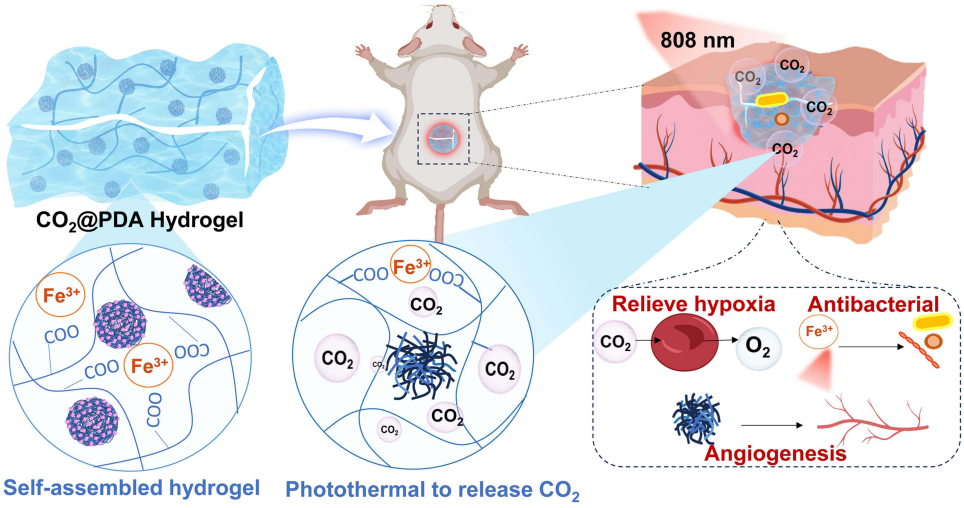

complex factors such as oxidative stress, tissue hypoxia, bacterial infection, and abnormal angiogenesis has become a clinical problem that needs to be solved urgently.[1] Designing a multifunctional reparative wound dressing that delivers O_2 while reducing the inflammatory response, inhibiting microorganisms, and promoting angiogenesis has become a hot research topic in skin wound treatment with significant application value.[2,3] Among many therapeutic methods, the transmission of CO_2 could be used as an alternative therapy to replace the high price and low solubility of pure O_2.[4] Based on the principle of the Bohr effect, when CO_2 is delivered to hypoxic wound tissue, it will activate hemoglobin by reducing the pH value of blood, resulting in more endogenous O_2 entering the injured tissue, providing necessary O_2 for tissue remodeling to accelerate wound healing.[5] It has been proved that hydrogel-coated carbon nanoparticles can effectively promote wound healing by responding to the photothermal release of CO_2 on demand.[6] However, for the complex environment of diabetic wounds, a multifunctional therapeutic strategy that can simultaneously exert antibacterial, antioxidant, and improve the hypoxic microenvironment is needed to promote wound healing effectively.

Hydrogel materials fit into the moist wound healing theory, facilitate gas exchange, and deliver biomolecules to promote tissue repair and regeneration. These have achieved great success and are widely used in wound dressings.[7] However, hydrogel dressings with complex compositions and complicated synthetic routes always raise concerns about biocompatibility and immunogenicity. New hydrogel dressings with simple synthesis, adjustable mechanical strength, and high biosafety are urgently needed. *Bletilla striata* polysaccharide (BSP), a natural component of traditional Chinese medicine with high biocompatibility, reduces inflammation and promotes vascular regeneration in the wound-healing process of diabetes.[8] More importantly, after it is modified into carboxymethyl *Bletilla striata* polysaccharide (CBSP), it can cross-link with metal ions such as Cu^{2+}, Fe^{3+} and self-assemble to form the hydrogel.[9] The hydrogel maintains the physiological activity of BSP and is endowed with a self-healing ability through the dynamic cross-linking network to adapt to the application of different wounds. Recently, polydopamine (PDA) has attracted significant attention in chronic wounds, attributed to its simple manufacturing process, high near-infrared ray (NIR) conversion efficiency, broad-spectrum photothermal bactericidal power, free radicals scavenging capacity, and good biocompatibility.[10] The PDA NPs loaded into the hydrogel will endow it with photothermal conversion response characteristics and enhance its antibacterial effect to promote healing.[11]

Current studies have explored the dynamic combination of *Bletilla striata* polysaccharide with borate ester bonds from borax to form pH and glucose-responsive hydrogels. This system additionally incorporates tannic acid-Fe^{3+} complexes as photothermal agents to enhance antibacterial effects.[12] Dopamine forms hydrogels through amide bonds with carboxyl groups on carboxymethylated *Bletilla striata* polysaccharide, enabling sustained antibacterial capability via

berberine delivery.[13] Another study involves coating CuO_2 nanoparticles with polydopamine and berberine, then incorporating them into oxidized *Bletilla striata* polysaccharide hydrogel crosslinked with hydroxypropyl trimethyl ammonium chloride chitosan, endowing the hydrogel with photothermal effects for enhanced antimicrobial activity in diabetic wound treatment.[14] Although these studies have applied polysaccharides or dopamine as formulation materials, their primary focus has been on enhancing antibacterial capacity through photothermal effects, with limited exploration in gas therapy for ameliorating hypoxic conditions in diabetic wounds, particularly regarding their application as delivery carriers for CO_2.

Herein, we proposed responsive hydrogels loaded with PDA NPs containing HCO_3^- by the electrostatic effect of Fe^{3+} (CO_2@PDA Hydrogel), which transported CO_2 in NIR controlled manner and promoted wound healing. Under near-infrared light irradiation, PDA NPs converted light energy into heat energy to promote the decomposition of HCO_3^- to generate a large amount of CO_2. The released CO_2 regulated the hypoxia microenvironment. The photothermal reaction of PDA NPs exerted an antibacterial effect and promoted the dissolution of hydrogels, which was conducive to the anti-inflammatory and vascular effects of CBSP. This study provided a feasible strategy for the multifunctional treatment of refractory wounds in diabetes Scheme1.

Materials and Methods

Materials

Fresh *Bletilla striata* was provided by Sichuan Kangyangjian Biotechnology Co. (Mianyang, China). Chloroacetic acid and ferric chloride ($FeCl_3$) were purchased from Sinopharm Chemical Reagent Co., Ltd (Shanghai, China). Dopamine hydrochloride (DA) was purchased from Sigma-Aldrich. Dulbecco's Modified Eagle's Medium (DMEM), trypsin (EDTA), Fetal Bovine Serum (FBS), Calcein-AM/PI Double Stain Kit, and Cell Counting Kit-8 (CCK-8) were purchased from Boster Biological Technology Co., Ltd (Wuhan, China). Reactive Oxygen Species (ROS) Assay Kit was purchased from Beyotime Biotechnology. Deionized water was used in all experiments.

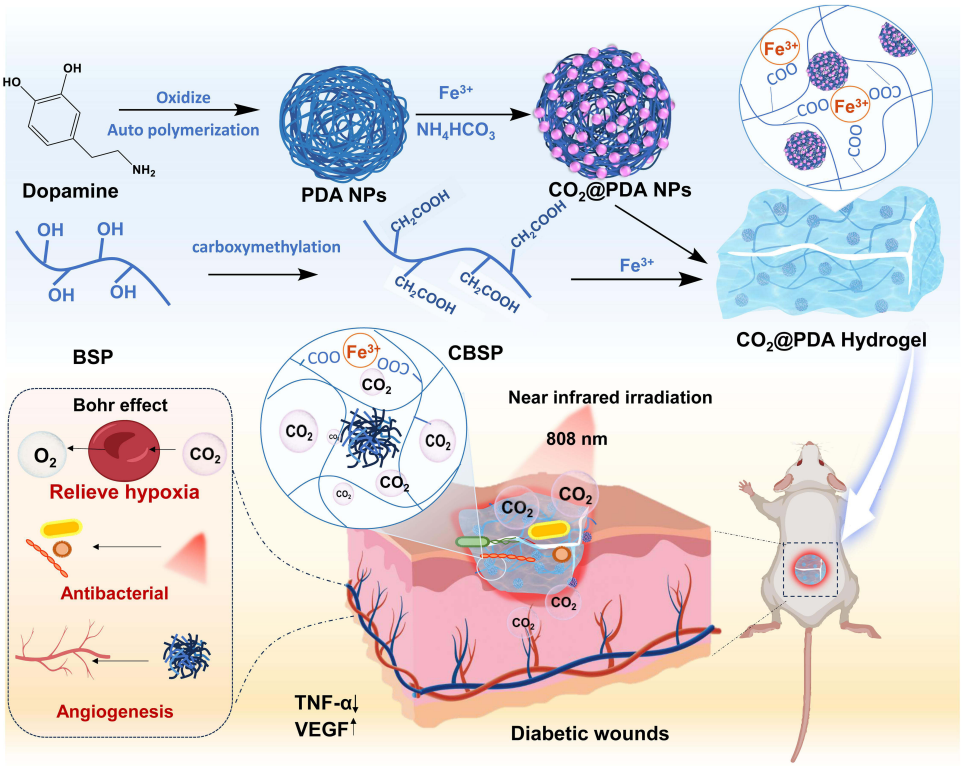

Scheme 1 Schematic Diagram of CO_2@PDA Hydrogel Releasing CO_2 in Response to Photothermal Effect to Accelerate Wound Healing in Diabetes.

https://doi.org/10.2147/IJN.S525172

NCTC clone 929 (L929 cells) was purchased from Shanghai Gaining Biological Technology Co., Ltd. (Shanghai, China).

Preparation of CO_2@PDA NPs

The preparation of PDA NPs followed the method of published literature with slight modifications.[15] First, anhydrous ethanol (20 mL), aqueous ammonia solution (1 mL), and water (deionized, 45 mL) were mixed under 100 rpm stirring for 0.5h. Subsequently, 5 mL DA solution (50 mg/mL) was added to the mixture and stirred for another 24 h. Eventually, after centrifugation and resuspension in deionized water (repeated 3 times), PDA NPs were obtained by freeze-drying.

The catechol structure on PDA NPs with characteristic intramolecular groups such as amine and carboxyl functional groups and catecholamines provide adequate sites for chelating metal ions. Therefore, PDA NPs were chelated with metal ion Fe^{3+} and adsorbed HCO^{3-} on the outer layer by electrostatic interaction to form CO_2@PDA NPs. First, Fe^{3+} was added to the above-prepared PDA NPs (pH 8.5 Tris buffer), stirred for 2 h, and purified by centrifugation with pure water to obtain PDA-Fe^{3+} NPs. The PDA-Fe^{3+} NPs were dispersed in water by sonication and added to NH_4HCO_3 solution (5 mm) under an ice bath to stand for 1 h. The NH_4HCO_3 was dropwise at 1 h intervals (4 times). After centrifugation and washing 3 times with 0.5 mm NH_4HCO_3 solution, the CO_2@PDA NPs were obtained by freeze-drying.[6]

Preparation of BSP and CBSP

The preparation of BSP was carried out as described in our previously reported literature.[16] In short, the dried *Bletilla striata* powder, after degreasing with ethanol and petroleum ether, was added to 40 times deionized water (m/v) and stirred at 70°C for 2 h. Then, sevag reagent was added to the above water extract concentrate to remove the protein, and then absolute ethanol was added to the concentration of 80% to precipitate it (v/v). The precipitate was left at 4°C overnight, washed successively with absolute ethanol, acetone, and diethyl ether, and dried at 40°C to constant weight. The BSP product was purified by DEAE-52 cellulose column and freeze-dried.

CBSP, a carboxymethyl-modified BSP, was synthesized according to the method previously reported by the research group.[9] Briefly, BSP was dissolved in a 20% NaOH solution under the cooling conditions of an ice water bath. Then, 30 mL of isopropanol was added to the above solution and stirred continuously for 0.5 h, followed by a slow addition of chloroacetic acid and stirring at 55°C for 1.5 h. The pH of the above-mixed solution was adjusted to 7.0, dialyzed, and lyophilized to obtain CBSP, which validated the structure by nuclear magnetic resonance spectroscopy and uniformity by High-Performance gel permeation chromatography (Supporting Information Figure S2).

Preparation of CO_2@PDA Hydrogel

The prepared CBSP was dissolved in deionized water to 100 mg/mL, then mixed with freshly prepared $FeCl_3$ solution to fabricate the CBSP/Fe^{3+} self-crosslinking hydrogel and named Hydrogel. Similarly, PDA NPs and $FeCl_3$ were added to the CBSP solution to prepare PDA Hydrogel. CO_2@PDA NPs were added to the CBSP solution to prepare CO_2@PDA Hydrogel. The composition of Hydrogel is given in Table S1.

Characterization of CO_2@PDA NPs and Related Hydrogels

The size, PDI value, and zeta potential of PDA NPs and CO_2@PDA NPs were determined by dynamic light scattering (DLS). The CO_2@PDA NPs, hydrogel, and CO_2@PDA hydrogel were freeze-dried, sprayed with gold, and characterized by a scanning electron microscope (SEM) to observe surface morphology (Zeiss Merlin Compact, Germany). The FTIR spectrum of DA, PDA NPs, CO_2@PDA NPs and related hydrogels was determined by the FTIR spectrometer (Japan) at the range of 4,000–500 cm^{-1}. The X-ray diffraction patterns of DA, PDA NPs, CO_2@PDA NPs, and related hydrogels were determined by an X-ray diffractometer (scan rate 4 min^{-1}) from angles of 5–60.

Rheology Properties, Self-Healing Behavior and Degradation of Hydrogels

The rheological properties of the different hydrogel samples were determined by a rheometer (DHR-1) under various conditions. The oscillating angular frequency sweep test investigated the properties of self-assembled hydrogels cross-linked with varying concentrations of Fe^{3+}. The storage modulus (G') and loss modulus (G") of the hydrogels were measured with angular frequency swept from 0.1 to 100 rad/s (10% strain, 25 ± 0.1°C). The rheological properties of CO_2@PDA hydrogels were determined by dynamic strain sweep frequency and cyclic strain tests. Dynamic strain scanning measurement frequency is 10 rad/s, and the applied strain is 1–1000%. The oscillatory strains were alternately switched from γ = 1% to γ = 300% in the cyclic strain tests. In addition, the self-healing performance of CO_2@PDA hydrogel is obtained by observing the appearance change after cutting the hydrogel into two halves after 30 min.

To determine the in vitro degradation rate of the hydrogels, the sterilised dried hydrogel and CO_2@PDA hydrogel were immersed in 30 mL PBS (pH = 7.4) at constant temperature (37°C) with shaking at 100 rpm. Then, at different time points (1, 2, 3, 4, 5, 6, 7 d), the hydrogels were taken out, irradiated with an 808 nm near-infrared laser for 10 min, washed with pure water 3 times, dried and weighted to define the degradation rate through the following equation:

$$\text{Degradation rate of hydrogel}(\%) = (W_0 - W_t)/W_0 \times 100\%,$$

W_t, the dry weights of the remaining hydrogels after degradation;
W_0, dry weights of the initial hydrogels.

Photothermal Properties and CO_2 Quantitation of CO_2@PDA Hydrogels

After irradiation of hydrogel, PDA hydrogels, and CO_2@PDA hydrogels with 808nm near-infrared laser, the thermal image is captured by the near-infrared thermometer to evaluate their photothermal conversion effect.[17] Briefly, hydrogel, PDA hydrogels, CO_2@PDA hydrogels (200 μL) were added to 1.5 mL centrifuge tubes containing 1.0 mL of deionized water and irradiated with an 808 nm near-infrared light laser for 10 minutes (2 W/cm^2). Simultaneously, the infrared thermal imager was adopted to monitor the temperature changes and capture their thermal images at 0, 2, 4, 6, 8, and 10 min. Subsequently, the photothermal stability of CO_2@PDA hydrogels was investigated using an on-off laser cycle by continuous irradiating and cooling four times.

After the CO_2@PDA Hydrogels convert light energy into heat energy, it promotes HCO_3^- to decompose into CO_2, and the released CO_2 reacts with calcium hydroxide to form calcium carbonate. The content of CO_2 is indirectly calculated based on calcium carbonate content.[6] A certain amount (0.5, 1, and 2 ppm) of CO_2@PDA hydrogels was added to an excess of calcium hydroxide aqueous solution (4 mm). The mixture is sealed and heated for 10 minutes (50°C). Subsequently cooled to 25°C, the precipitate was centrifuged and washed 3 times with deionized water to obtain calcium carbonate ($CaCO_3$). The $CaCO_3$ was dissolved in a 5% nitric acid solution and determined the Ca element content by ICP-AES.

Cytocompatibility and Hemolysis Assays of CO_2@PDA Hydrogels

The CCK-8 assay and living/dead cell staining were used to evaluate the cytocompatibility of CO_2@PDA hydrogels and their effects on cell growth. L929 cells were cultured in DMEM complete medium supplemented with 10% FBS and 1% penicillin-streptomycin and placed in a CO_2 incubator at 37°C. L929 cells were seeded into a 96-well plate at a rate of 5000 cells/well and culture overnight. Then, the medium was removed, and cells were, respectively, added to 100 μL fresh medium with sterilized Hydrogel, PDA Hydrogel, and CO_2@PDA Hydrogel and co-culture for another 24 h (1mg/mL). Then, the supernatants were removed from per well, and 100 μL CCK-8 reagent (10% v/v) was added and incubated for an additional 2 h. Eventually, the absorbance at 450 nm per well was measured by a microplate reader (Multiskan SkyHigh, ThermoFisher).

Cells Live/Dead stained by Calcein-AM/PI Double Stain Kit was carried out to evaluate the effect of hydrogel on cell proliferation. The L929 cells were seeded into a 48-well plate and culture overnight. The cells were incubated in a medium containing Hydrogel, PDA Hydrogel, and CO_2@PDA Hydrogel (1mg/mL) for 48 h. Then, after being washed with a sterile PBS solution, L929 cells were stained with Calcein-AM/PI dye for 30 min in the dark. Finally, the

fluorescence images of the cells were observed and collected under an inverted fluorescence microscope (Leica DM6 B, Germany).

The hemolytic test was used to estimate the biosafety of exogenous substances or materials in blood. The fresh rat blood was centrifuged at 3500 rpm for 5 min, resuspended in sterile PBS, and centrifuged and resuspended 5 times. Finally, the centrifuged red blood cells were prepared into a 5% suspension using PBS, resulting in a 5% erythrocytes suspension. Subsequently, Hydrogel, PDA Hydrogel, and CO_2@PDA Hydrogel were mixed with 500 μL diluted 5% erythrocytes in a tube and placed in a rocking shaker at 37°C for 1 h (100 rpm). After that, all samples were centrifuged and transferred 100 μL supernatant into a 96-well plate to detect the absorbance at 545 nm by a microplate reader.

Antioxidant, ROS Scavenging, and Antibacterial Effects of CO_2@PDA Hydrogels in vitro

The antioxidant properties of the Hydrogel, PDA Hydrogel, and CO_2@PDA Hydrogels were estimated by the DPPH radical scavenging test.[18] Hydrogel samples solution (2 mL) were dispersed in DPPH-ethanol solution (1:1) and incubated in the dark for 30 min. The wavelength of DPPH was scanned by a UV–vis spectrophotometer, and the scavenging of DPPH was calculated by the Eq. (1):

$$\text{DPPH scavenging}(\%)=(Abs_b - Abs_h)/Abs_b \times 100\% \quad (1)$$

Where Abs_b was the absorption of the blank (DPPH and ethanol) samples and *Absh* was the absorption of hydrogel samples (DPPH, ethanol, and hydrogel) at the wavelength of 517 nm, respectively (n = 3).

L929 cells (5×10^4/mL) were seeded in a 24-well plate and culture overnight. The medium was removed, and the cells were incubated in DMEM solution with a DCFH-DA fluorescent probe (10 μM) in the dark for 30 min. The positive control Rosup solution was treated with cells in the dark for 30 min to produce ROS rapidly after being treated with 1 mg/mL of Hydrogel, PDA Hydrogel, and CO_2@PDA Hydrogels for 30 min, respectively. The L929 cells were washed 3 times with PBS, and each sample's fluorescence intensity was measured by flow cytometry. The L929 cells were cultured and treated according to the above steps, incubated with a DCFH fluorescent probe, and co-incubated with the same drug dose in a confocal dish. The fluorescence intensity of cells was observed under the inverted fluorescent microscope.

Staphylococcus aureus (*S. aureus*) and *Escherichia coli* (*E. coli*) as the common bacteria on wounds were selected as bacterial models for antibacterial experiments, and the antibacterial ability of Hydrogel, PDA Hydrogel, and CO_2@PDA Hydrogels was evaluated by spread plate method. About 200 μL hydrogel samples were injected into the 48-well plate containing 200 μL bacterial suspension (10^6 CFU/mL). Each well was irradiated with near-infrared light for 10 minutes (808 nm, 2 W/cm^2). Then, 600 μL of liquid culture medium was added to the plate and incubated for 12 h in a constant temperature incubator (37°C). The culture medium plate without any bacteria was the blank sample. Subsequently, 100 μL suspension of each well was taken to assess the absorbance at 600 nm. Lastly, another 10 μL suspension was taken from each well and diluted with 1 mL PBS 3 times. About 100 μL diluent was applied to a solidified agar plate and incubated in an incubator for 16 h. After forming the bacterial community, viable colony units were photographed and counted.

Healing-Promoting Effect of CO_2@PDA Hydrogels on Diabetes Wounds

Male Sprague-Dawley rats (200 g) were obtained from SPF Biotechnology Co., Ltd (Beijing, China). All in vivo experiments were carried out under the guidelines approved by the Center for Experimental Animals (SYXK(Chuan)2024–0216), Southwest Minzu University, and performed by the approved procedures of the Institutional Animal Care and Use Committee (IACUC) of Sichuan Province, with permission certificate registration number (SMU-202401015).

Male Sprague-Dawley rats were given a standard chow diet and water with a 12-h light/dark cycle for 7 days before any experimental procedures. The diabetic rat model was established by intraperitoneal injection of streptozotocin-citrate buffer at 110 mg/kg. After their blood glucose levels ≥16.8 mmol/L, the mice were regarded as diabetic and used for *in-vivo* studies. After anesthesia with 2% isoflurane (0.41mL/min at 4L/min Fresh gas flow), the rats were shaved on the

back, and a circular wound with a diameter of 10 mm was cut using scissors. The depth of the wound reached the muscle layer, forming a full-thickness skin wound model in rats. Then, 50 μL of *E. coli* solution (10^8 CFU/mL) was attached to the wound surface for 24 h to form the bacteria-infected wound. Except for the control group, the wounds of each rat were covered with the hydrogel samples and under irradiation (808 nm) for 10 min, respectively. Simultaneously, the temperature change of the wound area was recorded by the infrared thermometer. The recovery of wounds on 3, 7, and 14 days were photographed and measured by the Image J software.

Wound Histology and Immunohistochemistry Analysis

After 14 days of treatment, the rats were euthanized by intraperitoneal injection of pentobarbital sodium solution (150mg/kg). The wound tissue from the original modelling site was cut off and fixed in a 4% buffered paraformaldehyde solution. After dehydration, it was embedded in paraffin. The embedded tissues were cross-sectioned into 5 μm-thick slices using a microtome, and the slices were stained with hematoxylin–eosin (H&E) reagents and Masson trichrome separately. In addition, after dewaxing and hydration, the slices were incubated overnight with TNF-α and VEGF antibodies at 4°C, washed with PBS, and then incubated with secondary antibodies at room temperature for 30 min. After washing, the slices were sealed for observation and image acquisition under a microscope. Semi-quantitative statistical analysis was performed using ImageJ.

Statistical Analysis

The data were presented as mean ± standard deviation. GraphPad Prism 8 software was used to perform one-way ANOVA on multiple data groups in the study to determine significant differences. The level of statistical significance was set to $*P < 0.05$.

Results and Discussion

Preparation and Characterization of CO_2@PDA NPs

The ability of the hydrogel to release CO_2 depends on the photothermal conversion performance of polydopamine nanoparticles, so the key point of this study is to prepare polydopamine nanoparticles that adsorb HCO^{3-}. As shown in Figure 1A, dopamine (DA) was self-polymerized under oxidizing conditions to form polydopamine nanoparticles (PDA NPs). Then, the catechol structure on the PDA NPs provided effective sites for chelating metal ions, starting with the complexation of Fe^{3+} by PDA NPs and binding ammonium bicarbonate by electrostatic adsorption to generate nanoparticles with HCO_3^- (CO_2@PDA NPs). The characteristics of PDA NPs determined by DLS include a particle size of 218 ± 2.54 nm, PDI of 0.186, and Zeta potential of −22.8 ± 2.05 mV (Supplementary Material Figure S1A and B). After modification, the characterization of CO2@PDA NPs showed a particle size of 226.3 ± 3.65 nm. PDI of 0.156, and Zeta potential of −15.5 ± 2.46 mV (Figure 1B). These results indicated that the binding of Fe^{3+} and HCO^{3-} increased the surface potential of CO_2@PDA NPs, but the change in particle size is relatively small.

The SEM image of the CO_2@PDA NPs showed a spherical shape, as shown in Figure 1C, but due to the influence of freeze-drying, the nanoparticles aggregate with each other. To demonstrate the successful synthesis of PDA and the effective loading of HCO^{3-} on PDA NPs, the FTIR spectra of DA, PDA NPs, and CO_2@PDA NPs were measured. As shown in Figure 1D, the broad peak at around 3400 cm^{-1} represents the stretching vibration peak of the hydroxyl group, 1610 and 1420 cm^{-1} are the stretching vibration absorption peaks of the benzene ring, 1280 cm^{-1} are the stretching vibration peaks of C-O and 1350 cm^{-1} aer the O-H deformation vibration peaks. PDA has distinct representative peaks at 1610,1420, and 1350 cm^{-1} compared to DA, which proves the successful synthesis of PDA NPs. The increase in peak intensity at about 1280 cm^{-1} for CO_2@PDA NPs compared to PDA NPs was due to the addition of NH_4HCO_3, indicating the successful loading of HCO_3^- ions on PDA. XRD further verified the crystal structure changes of the CO_2@PDA NPs.[6] The XRD results of nanoparticles are shown in Figure 1E, comparing with DA, PDA NPs, and CO_2@PDA NPs had no sharp diffraction between 15° and 35°, indicating that both are amorphous structures. The XRD results confirm the successful preparation of the CO_2@PDA NPs, but their ability to release CO_2 needs further investigation.

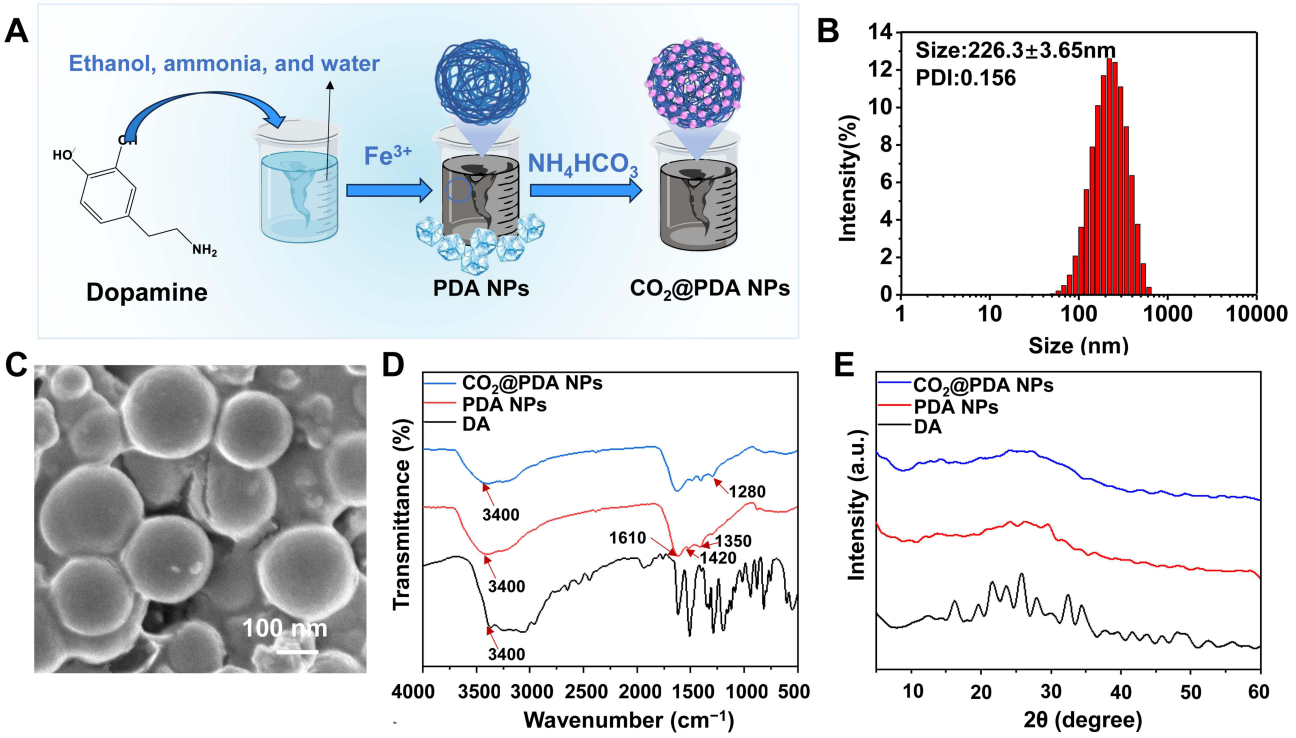

Figure 1 Preparation and characterization of CO_2@PDA NPs. (**A**) Schematic diagram of CO_2@PDA NPs. (**B**)Particle and PDI of CO_2@PDA NPs. (**C**)SEM of CO_2@PDA NPs. (**D**) FTIR spectra of DA, PDA NPs, and CO_2@PDA NPs. (**E**) XRD of DA, PDA NPs, and CO_2@PDA NPs.

Preparation and Characterization of CO_2@PDA Hydrogel

Bletilla striata polysaccharide has a good ability to promote wound healing and has obvious viscosity due to its large number of hydroxyl groups.[19] However, its ability to form hydrogel alone is limited, and it is often used together with chitosan, sodium alginate, and other macromolecular substances as a hydrogel matrix. Replacing the hydroxyl group of *Bletilla striata* polysaccharide with the carboxymethyl group can enhance the hydrogen bonding between molecular chains, help to bond a large number of water molecules, facilitate the formation of hydrogel, and show stronger moisture absorption and moisture retention ability.[20] This study obtained CBSP from *Bletilla striata* polysaccharides through etherification and confirmed the successful synthesis of CBSP through 13C-NMR, and carboxyl content determination (Supporting Information Figure S2A and B).

The rich carboxyl groups in CBSP are crosslinked with Fe^{3+} to form a porous network hydrogel. Fe^{3+} has been introduced into the CO_2@PDA NPs formation process. The CBSP and CO2@PDA NPs mixture can also spontaneously form hydrogels (Figure 2A). As shown in Figure 2C, with the increase of Fe^{3+} content, the pore diameter and porosity of the hydrogel formed gradually decrease (Figure 2B), indicating that Fe^{3+} is the key factor in regulating the structural compactness of the hydrogel. Therefore, Fe^{3+} contained in CO_2@PDA NPs form porous network hydrogels with CBSP, and spherical nanoparticles are embedded on the surface. This result confirmed that CBSP and CO_2@PDA NPs cross-link through coordination bonds to form a porous and soft hydrogel, which is conducive to matching the amorphous wound shape of diabetes.

The rheological tests provided fast and sensitive methods to evaluate the mechanical properties of hydrogels. As shown in Figure 2D, the G′ of the hydrogel gradually increased with the increase of frequency, while the G" decreased with the rise in frequency, indicating that the elasticity of the hydrogel increases with the increase of frequency, while the viscosity decreases. With the increase in the amount of Fe^{3+}, the elasticity of the hydrogel was increased, which is conducive to forming a stable hydrogel. The intermediate concentration of Fe^{3+} was selected to prepare CO_2@PDA Hydrogel further to have appropriate elasticity and viscosity, which is conducive to applying irregular wounds. The self-healing ability of CO_2@PDA Hydrogel was evaluated by a quantitative method such as a dynamic strain sweep test. The

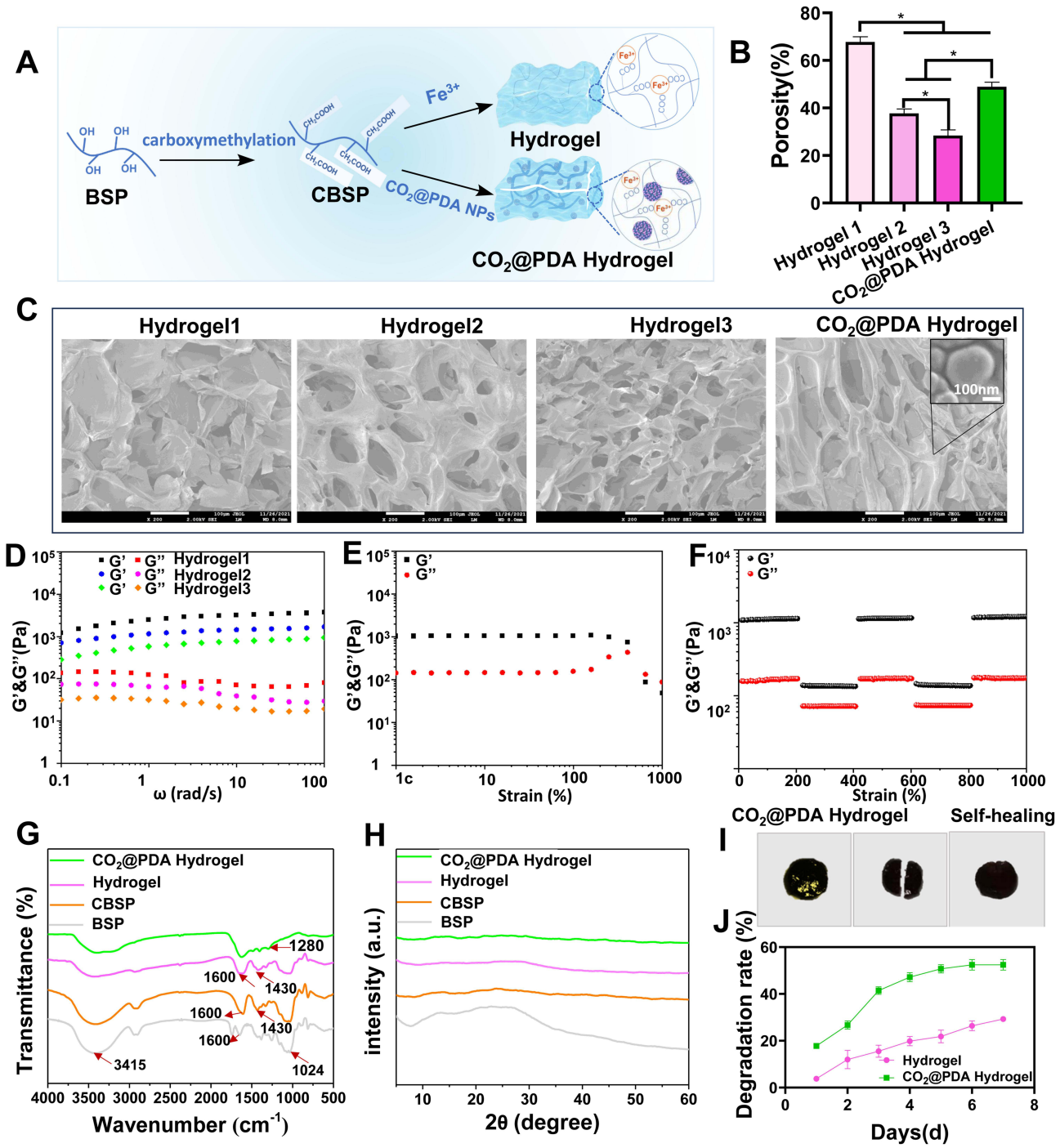

Figure 2 Preparation and characterisation of CO_2@PDA Hydrogel. (**A**) Schematic diagram of hydrogel preparation. (**B**) The porosity of CO_2@PDA Hydrogel and Hydrogels crosslinked by different Fe^{3+}. (C)SEM of CO_2@PDA Hydrogel and Hydrogels crosslinked by different Fe^{3+}. (**D**) Rheological properties of Hydrogels crosslinked by different Fe^{3+}. (**E**) Dynamic strain sweep test of CO_2@PDA Hydrogel. (**F**) Cyclic strain test of CO_2@PDA Hydrogel. (**G**) FTIR spectra. (**H**) XRD spectra. (**I**) Self-healing ability of CO_2@PDA Hydrogel. (**J**) Degradation capacities of the hydrogels in PBS with pH 7.4 at 37 °C. Data are presented as the mean ± SEM. *P < 0.05.

results in Figure 2E indicated that the gel-sol transition crossover point is above 300% of strain. This suggests that the internal network is disrupted when the strain exceeds 300%, and the CO_2@PDA Hydrogel undergoes liquefaction.

The self-healing ability of CO_2@PDA Hydrogel with continuous hydrogel could quickly become whole, showing the properties of liquid and vividly showing the self-healing characteristics of the hydrogel. The self-healing property of hydrogels is attributed to the dynamic reversibility of metal coordination bonds, which enables them to reconstruct their

https://doi.org/10.2147/IJN.S525172

original structure after fracture. The self-healing property of hydrogel enables it to respond to various mechanical pulling when applied to wounds, providing a strong guarantee for continuous protection of wounds from secondary pulling.[21] Therefore, CO_2@PDA Hydrogel adapts to the dynamic changes of wounds due to its excellent self-healing properties when applied to wound healing.

According to the amount of Fe^{3+} contained in CO_2@PDA Hydrogel, the Hydrogel crosslinked with CBSP by the same amount of Fe^{3+} is prepared. FTIR spectra were used to determine the changes in chemical bonds in BSP, CBSP, Hydrogel, and CO_2@PDA Hydrogel, as shown in Figure 2G. In the chemical structure of BSP, the peak at 3415 cm^{-1} is a strong absorption peak of O-H, and the peak at 1024 cm^{-1} is a typical feature of the pyranoside configuration.[22] Compared with BSP, the FTIR spectrum of CBSP shows new strong absorption peaks around 1600 and 1430 cm^{-1}, which were caused by the stretching vibration of carboxymethyl C=O. The change in characteristic peaks indicated the successful introduction of carboxymethyl groups into BSP polysaccharide molecules, consistent with the ^{13}C-NMR results in Figure S2. Due to the interaction between Fe^{3+} and -COOH, the blue shift of the O-H stretching peak and the weakening of the -COOH characteristic peak at 1600 cm^{-1} appear in Hydrogel, which indicates the effective complexation of Fe^{3+} with the polysaccharide molecule. In the CO_2@PDA hydrogel, the configuration of pyranoside from BSP was completely concealed, and a characteristic peak of 1280 cm^{-1} from PDA NPs appeared, indicating that the PDA NPs were successfully encapsulated in the CO_2@PDA hydrogel. The XRD results of BSP, CBSP, Hydrogel, and CO_2@PDA Hydrogel were shown in Figure 2H. Only one broad peak is observed in the BSP curve, proving both are amorphous materials. Similarly, no new peaks appear in the CBSP, Hydrogel, and CO_2@PDA Hydrogel, presenting an amorphous structure.

The hydrogel sample will gradually dissolve over time, providing favourable conditions for the release of the loaded drugs. As shown in Figure 2J, after 808 nm near-infrared laser irradiation, the degradation rate of the photothermal-responsive CO_2@PDA Hydrogel significantly increased. By the 7th day, the degradation rate of the CO_2@PDA Hydrogel was as high as 52.44%, while that of the Hydrogel was only 29.27%, indicating that laser irradiation had effectively promoted the degradation of the hydrogel. In previous reports, precursor drugs using carbon nanoparticles to adsorb CO_2 were mixed with Pluronic F127 for on-demand delivery of CO_2. However, the carbon nanoparticles used in the system are difficult to completely degrade and also have certain toxicity. But all materials in this study are safe, non-toxic, and have good degradation performance, providing a guarantee for the safe application of drugs.[6]

NIR-Photothermal Performance of CO_2@PDA Hydrogel

The photothermal effect stimulates local microcirculation blood flow, inhibits bacteria, and reduces inflammation to promote wound healing by converting light into heat.[23] The efficacy of photothermal conversion is the starting force of the CO_2@PDA Hydrogel to release CO_2.[24] The photothermal properties of the CO_2@PDA Hydrogel samples were studied by measuring the temperature change, and CO_2 release after the hydrogel samples were irradiated with an NIR laser (808nm). The photothermal images of different hydrogels are shown in Figure 3A. After irradiation for 10 min, the temperature of PDA Hydrogel and CO_2@PDA Hydrogel were increased by approximately 33.6 and 33.1°C, respectively, which was significantly higher than that of Hydrogels by 2.3°C. These results indicate that the good photothermal conversion ability of PDA hydrogels and CO_2@PDA Hydrogel is due to the presence of PDA NPs. The heat change curve in Figure 3B showed the same trend. In addition, the photothermal stability of CO_2@PDA Hydrogel was investigated by laser on/off experiments with 4 cycles. As shown in Figure 3C, the ramp-up ability of CO_2@PDA Hydrogel did not change significantly before and after, indicating that it had good photothermal stability and repeatability and can be used as an excellent photothermal conversion material. The amount of CO_2 released from the CO_2@PDA Hydrogel was shown in Figure 3D. The results showed that the amount of CO_2 released from the hydrogel increases with the amount of CO_2@PDA Hydrogel. This proved that the hydrogel effectively releases CO_2 through NIR laser response, providing a feasible strategy for improving the hypoxic environment of diabetes wounds.

Cytocompatibility and Hemolysis Assays of CO_2@PDA Hydrogels

The cytotoxicity test was used to determine the biocompatibility of CO_2@PDA Hydrogel and provided the basis for determining its dosage in L929 cells.[25] As shown in Figure 4A, after co-incubation with cells for 1 day, there was no

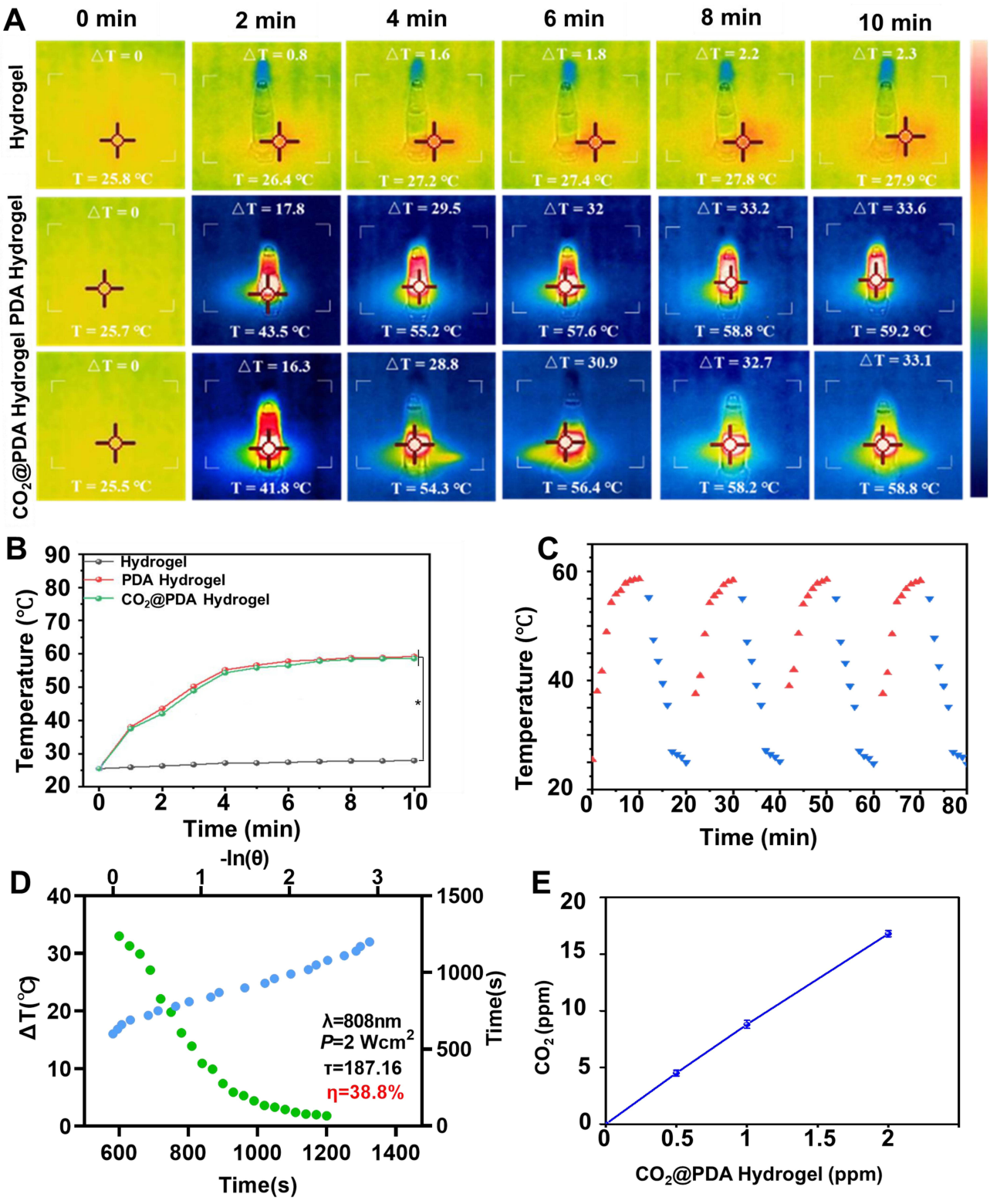

Figure 3 The photothermal effect of CO_2@PDA Hydrogel. (**A**) Photothermal images of Hydrogel, PDA Hydrogel, and CO_2@PDA Hydrogel. (**B**) The heat change curve of Hydrogel, PDA Hydrogel, and CO_2@PDA Hydrogel. (**C**) Four irradiation-cooling cycles of CO_2@PDA Hydrogel. (**D**) The photothermal conversion rate of CO_2@PDA Hydrogel. (**E**) the amount of CO_2 released from CO_2@PDA Hydrogel. Data are presented as the mean ± SEM. *P < 0.05.

https://doi.org/10.2147/IJN.S525172

discernible difference in the relative survival rates of Hydrogels, PDA Hydrogels, and CO_2@PDA Hydrogels. The cell survival rates remained essentially constant, exceeding 90%, indicating that the formulated hydrogels had no cytotoxic effects. Moreover, the impact on cell proliferation was visually assessed by live/dead staining assay. As shown in Figure 4B, after 3 days of co-culture in the hydrogel extract, all experimental groups had a cell proliferation-promoting effect. These results may be because BSP is a natural polysaccharide with good biocompatibility after being modified into CBSP, and the hydrogel prepared with CBSP as the main matrix also has the effect of promoting cell proliferation. Overall, the cytocompatibility experiments revealed that the prepared hydrogels (1mg/mL) had good cytocompatibility and could be a promising candidate for tissue repair.

The biocompatibility of a material is crucial before it is used in biomedical applications. As a wound dressing, hydrogel comes in contact with blood and skin trauma from its initial application scenario of stopping bleeding to promoting wound healing.[8] Therefore, the hemolysis test on hydrogel is a classic test to evaluate its safety as a biomaterial.[26] As shown in Figure 4C, the hemolysis rate results of hydrogel groups, including hydrogel, PDA hydrogel, and CO_2@PDA Hydrogel, similar to the PBS treatment group incubated with red blood cell suspension, were lower than 2%. Compared with the hemolysis group of water treatment, the hemolysis rate of each Hydrogel group was significantly lower than that of the water treatment group ($P < 0.05$). The intuitive result is shown in Figure 4D. These results indicate that our prepared pre-materials and composite hydrogels have good erythrocyte compatibility, no hemolytic effect on erythrocytes, and good hemocompatible.

Antioxidant and ROS Scavenging Effects of CO_2@PDA Hydrogels

Hyperglycemia in diabetic wounds will hinder the expression of chemokines, block the process of monocyte recruitment in the wounds, slow the clearance of pathogens by neutrophils, and increase oxidative stress in the wounds. Continuous oxidative stress promotes the aging of fibroblasts and other cells, which is extremely detrimental to wound healing.[27] The excellent antioxidant properties of natural polysaccharides enable them to eliminate excessive ROS in wounds, avoid ROS-induced excessive inflammation, and accelerate the wound healing process.[28] The DPPH radical scavenging assay is a recognized quantitative analysis method for evaluating the antioxidant activity in vitro of drugs. The antioxidant results of Hydrogels, PDA Hydrogels, and CO_2@PDA Hydrogels by the DPPH method are shown in Figure 5A. The Hydrogels have a DPPH scavenging efficiency of 27% (0.5mg/mL), indicating that Hydrogel has a limited scavenging effect on DPPH free radicals. PDA is a type of melanin biomimetic material with excellent antioxidant properties, widely

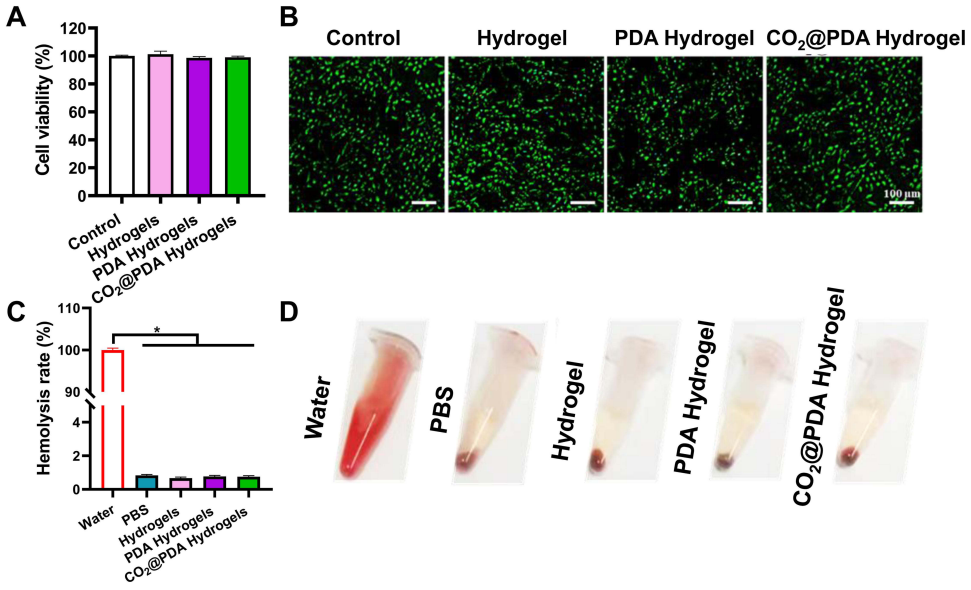

Figure 4 Cytocompatibility and hemolysis assays of CO_2@PDA hydrogels. (A)Cell viability of Hydrogel, PDA Hydrogel, and CO_2@PDA Hydrogel. (**B**) Live/dead cell images of different Hydrogels. (**C**) The hemolysis rate. (**D**) The hemolysis images. Data are presented as the mean ± SEM. *P < 0.05.

used in the field of biomedicine by clearing ROS. Therefore, compared with Hydrogel, PDA Hydrogels and CO_2@PDA Hydrogels loaded with PDA nanoparticles have significantly increased antioxidant activity ($P < 0.05$). However, there was no significant difference between PDA Hydrogels and CO_2@PDA Hydrogels in the antioxidant effect, indicating that the antioxidant effect of CO_2@PDA Hydrogels was mainly attributed to PDA NPs.

The scavenging of excessive intracellular ROS is an effective way to promote wound healing. The flow cytometry results are shown in Figure 5B. Hydrogels, PDA Hydrogels, and CO_2@PDA Hydrogel reduced the fluorescence produced by the excessive ROS caused by the rosup solution, and CO_2@PDA Hydrogel has the strongest removal effect ($P < 0.05$). The results obtained by fluorescence microscopy are shown in Figure 5C, which is consistent with the flow cytometry results. The ROS fluorescence was generated after the positive drug stimulation in the control group,

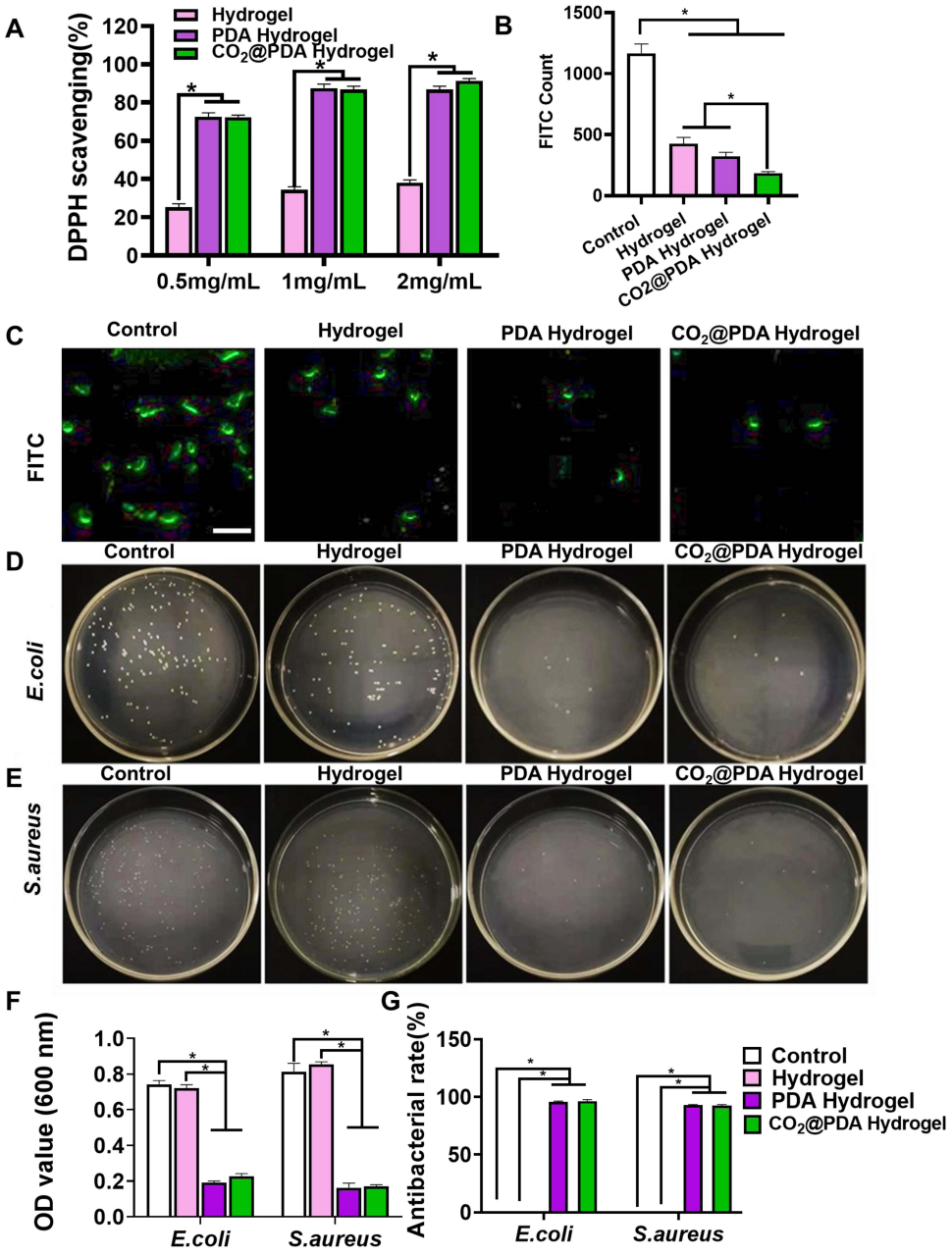

Figure 5 The antioxidant, ROS scavenging, and antibacterial effects of CO_2@PDA Hydrogel in vitro. (**A**) DPPH scavenging effect. (**B**) ROS scavenging effect in L929 cells. (**C**) Fluorescent image of ROS. (**D**) Image of *S. aureus*. on agar plates (**E**) Image of *E. coli*. on agar plates. (**F**) OD results of the bacterial suspensions. (**G**) The antibacterial of different hydrogels. Data are presented as the mean ± SEM. *P < 0.05.

https://doi.org/10.2147/IJN.S525172

while the ROS scavenging effect of varying degrees appeared after hydrogel treatment. These results are mutually verified with the results of the DPPH experiment, confirming that CO_2@PDA Hydrogel promoted the repair process by scavenging ROS in wound repair.

Antibacterial Effect of CO_2@PDA Hydrogel

Bacterial infection is one of the serious complications that affect wound healing and tissue regeneration. It may cause long-term chronic inflammatory reactions, leading to delayed wound healing. BSP is often used as the matrix of hydrogel to load antibacterial drugs, such as silver nanoparticles,[29] CuO nanoparticles,[14] berberine,[30] etc, and the antibacterial effect is obtained through the gradual release of these drugs. In addition, photothermal antibacterial therapy has also become an emerging method of bacterial inhibition, with the advantages of precise treatment, few side effects, and high efficacy. PDA NPs with photothermal effect were loaded into CBSP hydrogel, and their antibacterial results were shown in Figure 5D and E. After 10 min of NIR radiation on the samples, the Hydrogel group did not show the potential to inhibit the bacteria in *S. aureus* or *E. coli*. The PDA Hydrogel and CO_2@PDA Hydrogel had a good destructive effect on the bacteria, which may be directly related to the ability of PDA NPs to convert light energy into heat energy after irradiation and achieve the antibacterial effect through temperature rise. The OD results of the bacterial suspensions are shown in Figure 5F. Whether in *S. aureus* or *E. coli*, the OD value of the Hydrogel group was equivalent to that of the control group. In contrast, the OD value was significantly reduced in PDA Hydrogel and CO_2@PDA Hydrogel ($P < 0.05$), showing good antibacterial ability. As shown in Figure 5G, the inhibition rate of both PDA Hydrogel and CO_2@PDA Hydrogel on *E. coli* and *S. aureus* reached over 90%. The antibacterial results showed that the antibacterial effect of CO_2@PDA Hydrogel was mainly due to its photothermal properties, and it had advantages in treating complex infectious wounds.

Healing-Promoting Effect of CO_2@PDA Hydrogel on Diabetes Wounds

Diabetic wounds are typical chronic non-healing wounds. This section is used to verify the in vivo effect of CO_2@PDA Hydrogel on wound healing in diabetic rats by establishing a diabetic rat-infected wound model. The previous study showed that NIR irradiation was beneficial to wound healing.[31] To keep the variables consistent, all groups were treated with NIR during the experiment, and the hydrogel dressing was changed every 3 days. Thermal images of rats treated with CO_2@PDA Hydrogel after NIR irradiation are shown in Figure 6D. The temperature in the CO_2@PDA Hydrogel group rapidly increased up to 56.1°C after 5 min of NIR laser irradiation, consistent with the in vitro results, which proved that CO_2@PDA Hydrogel had good photothermal conversion performance and provided a guarantee for effective treatment of bacterial infections in vivo.

As the most intuitive evaluation indicators, wound area and appearance are used to assess the wound-healing effect of each group.[32] Representative pictures of the wounds in each group at the same time interval were shown in Figure 6A. After 14 days of treatment, the wounds in the control group were red but not fully healed. The wounds in the Hydrogel group were slightly red, while those in groups PDA Hydrogel and CO_2@PDA Hydrogel were fully healed. The morphological changes of the wound were shown in Figure 6B, and quantitative analysis was shown in Figure 6C. Compared with the control group, the healing degree of PDA Hydrogel and CO_2@PDA Hydrogel was significantly better, and the wound healing ability of CO_2@PDA Hydrogel was the strongest ($P < 0.05$). The results showed that the healing effect of CO_2@PDA Hydrogel was not only due to the sterilization effect of the photothermal but also due to the effect of released CO_2 from CO_2@PDA Hydrogel to improve the hypoxic environment of the wound.

H&E staining sections can observe granulation tissue, inflammatory cells, and re-epithelialization.[33] As shown in Figure 6E, the control group had a lower degree of re-epithelialization of the injured area tissue and no skin accessory structures, such as hair follicles and sebaceous glands. As shown in Figure 6E, the control group had a lower degree of re-epithelialization of the injured area tissue and no skin accessory structures. In the Hydrogel group, the re-epithelialization of the wound was more obvious, but there was a small amount of inflammatory cell infiltration in the newly healed wound tissue. In the PDA Hydrogel group, a small number of sebaceous glands and other tissues appeared at the wound healing sites. In the CO_2@PDA Hydrogel, newly healed wounds of the CO_2@PDA Hydrogel groups, more

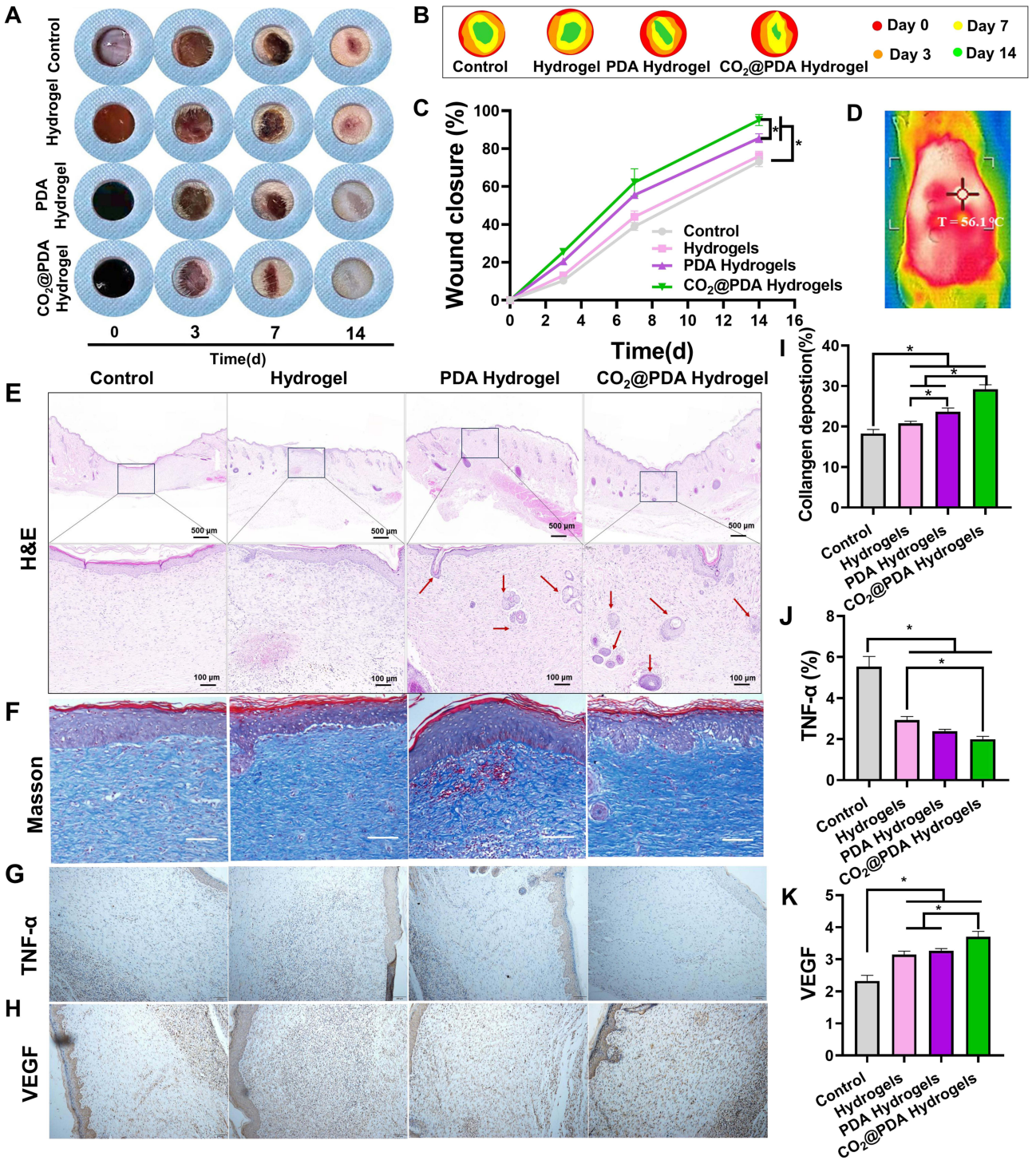

Figure 6 Healing-promoting effect of CO_2@PDA Hydrogel on diabetes wounds. (**A**) Wound images on 0, 3, 7, and 14 days. (**B**) The morphological changes of the wound. (**C**) Quantitative analysis of wound area. (**D**) Photothermal images of rat wounds after NIR irradiation. (**E**) H&E tissue section. (**F**) Masson tissue section. (**G**) Immunohistochemistry of TNF-α. (**H**) Immunohistochemistry of VEGF. (**I**) Collagen deposition. (**J**) The amount of TNF-α. (**K**) The amount of VEGF. Data are presented as the mean ± SEM. *P < 0.05.

skin accessory structures appeared, and the degree of re-epithelialization was higher, indicating that CO_2@PDA Hydrogel is more conducive to promoting wound healing and restoring normal tissue structure of the skin.

Collagen deposition was important in skin contraction, re-epithelialization, and initial dermal construction.[34] Collagen deposition in the skin after 14 days of treatment was evaluated by Masson staining in Figure 6F, and CO_2@PDA

https://doi.org/10.2147/IJN.S525172

Hydrogel-treated skin tissues showed substantial deposition of collagen fibers, which were significantly thicker, denser, and more directionally aligned, with improved extracellular matrix reconstruction and tissue remodeling. As in Figure 6I, statistical analysis found that the amount of collagen deposition in CO_2@PDA Hydrogel was significantly higher than in other groups ($P < 0.05$). The results showed that CO_2@PDA Hydrogel could promote collagen deposition to accelerate tissue remodeling.

After hemostasis, the wound enters the inflammatory stage, promoting the proliferation and differentiation of immune cells by releasing inflammatory factors. Differentiated macrophages engulf necrotic tissue and pathogens and release signaling factors to rebuild the wound tissue. However, if the wound is heavily infected and the inflammatory stage is not controlled, it will ultimately lead to delayed wound healing.[35] TNF-α, IL-1β, IL-10, and other typical pro-inflammatory factors can reflect the degree of wound inflammation.[36] As shown in Figure 6G and J, CO_2@PDA Hydrogel significantly reduced the content of TNF-α in the tissue ($P < 0.05$), indicating CO2@PDA Hydrogel promoted the wound to pass through the inflammatory stage and accelerated the wound healing process.

Activating angiogenesis was indispensable for maintaining regenerating tissue, allowing adequate nutrient and oxygen supply, and promoting cytokine transport and cell migration. VEGF promotes angiogenesis, stabilizes immature vessels, and plays an important role in angiogenesis.[37] As shown in Figure 6H and K, the distribution of VEGF is highest in CO_2@PDA Hydrogel group tissue. It is worth noting that VEGF in CO_2@PDA Hydrogel tissue was significantly higher than that in the PDA Hydrogel group, indicating that the released CO_2 from CO_2@PDA Hydrogel has a major promoting effect on vascular remodeling. In the rat diabetes wound model group, the wound closure rate, inflammatory level (H&E and TNF-a), collagen deposition, and vascular reconstruction (VEGF) were comprehensively evaluated the ability of CO_2@PDA Hydrogel to promote wound healing under near-infrared radiation, emphasizing its potential application in refractory chronic wounds.

Conclusion

In this work, a multifunctional photothermal self-healing hydrogel that can release CO_2 was designed to treat chronic wounds of diabetes based on the microenvironment regulation strategy of anti-hypoxia, anti-bacterial, and antioxidant synergistic effects. The hydrogel system exhibited good self-healing properties and adjustable mechanical strength due to dynamic metal coordination bonds and the proportion of components. In the PDA Hydrogel and CO_2@PDA Hydrogel groups, introducing PDA-based materials gave the gel significant photothermal effects and endowed the system with sustained antibacterial and free radical scavenging abilities and the capacity to release CO_2. In addition, this type of hydrogel demonstrated good cytocompatibility and hemocompatibility, and CO_2@PDA Gel healed well in a full-layer wound defect model. In summary, by rationally engineering the functional building blocks, PDA nanoparticles carrying CO_2 source were loaded into a coordination hydrogel system formed by natural polysaccharides and Fe^{3+} to achieve near-infrared controlled CO_2 release and accelerate the repair of refractory diabetes bacterial wounds. This study provides a practical, promising, powerful and orderly combined treatment strategy for treating infected wounds in diabetes.

Abbreviations

BSP, *Bletilla striata* polysaccharide; CBSP, *Bletilla striata* polysaccharide; PDA, Polydopamine; NIR, Near-infrared ray; FBS, Fetal bovine serum; CCK-8, Cell Counting Kit-8; ROS, Reactive Oxygen Species; L929 cells, NCTC clone 929; DLS, Dynamic light scattering; SEM, Scanning electron microscope; H&E, Hematoxylin-eosin.

Funding

This work was supported by National Natural Science Foundation of China (No.82404877, No.82474353), Natural Science Youth Foundation of Sichuan Province (No.2024NSFSC1685), Southwest Minzu University Research Startup Funds (No.RQD2024020), Fundamental Research Funds for Central Universities of Southwest Minzu University (No. ZYN2024034), Special research project of the Sichuan Provincial Administration of TCM (No.2023MS621), and Scientific and Technological Innovation Team for Qinghai-Tibetan Plateau Research in Southwest Minzu University (No.2024CXTD23).

Disclosure

The authors report no conflicts of interest in this work.

References

1. Liu P, Xiong Y, Chen L, et al. Angiogenesis-based diabetic skin reconstruction through multifunctional hydrogel with sustained releasing of M2 Macrophage-derived exosome. *J Chem Eng*. 2022; 431:132413.
2. Liang YP, He JH, Guo BL. Functional hydrogels as wound dressing to enhance wound healing. *ACS NANO*. 2021;15(8):12687–12722. doi:10.1021/acsnano.1c04206
3. Cai M, Liu Z, Sun X, et al. Advances in the development of medical dressings for the treatment of diabetic foot wounds. *Chem Eng J*. 2024;498.
4. Ghaffari-Bohlouli P, Jafari H, Okoro OV, et al. Gas therapy: generating, delivery, and biomedical applications. *SMALL METHODS*. 2024;8(8). doi:10.1002/smtd.202301349
5. Rivers RJ, Meininger CJ. The tissue response to hypoxia: how therapeutic carbon dioxide moves the response toward homeostasis and away from instability. *Int J Mol Sci*. 2023;24(6):5181. doi:10.3390/ijms24065181
6. Xie G, Zhou N, Gao Y, et al. On-demand release of CO2 from photothermal hydrogels for accelerating skin wound healing. *Chem Eng J*. 2021;403:126353. doi:10.1016/j.cej.2020.126353
7. Markovic MD, Spasojevic PM, Pantic OJ, Savic SI, Savkovic MMS, Panic VV. Status and future scope of hydrogels in wound healing. *Drug Deliv Sci Technol*. 2024;98.
8. Li XM, Bai LM, Zhang XW, Fang QW, Chen G, Xu G. Application of *Bletilla striata* polysaccharide hydrogel for wound healing among in diabetes. *Colloids Surf B Biointerfaces*. 2024;241.
9. Ma ZH, Li YH, Lv JY, et al. Construction and assessment of carboxymethyl *Bletilla striata* polysaccharide/polyvinyl alcohol wet-spun fibers load with polydopamine@metformin microcapsules. *Drug Deliv Sci Technol*. 2022;71.
10. Khalek MAA, Abdelhameed AM, Gaber SAA. The use of photoactive polymeric nanoparticles and nanofibers to generate a photodynamic-mediated antimicrobial effect, with a special emphasis on chronic wounds. *Pharmaceutics*. 2024;16(2):229.
11. Xu QT, Su W, Huang CL, et al. Multifunctional polysaccharide self-healing wound dressing: NIR-responsive carboxymethyl chitosan/quercetin hydrogel. *Adv Healthcare Mater*. 2024.
12. Hu Z, Zhao K, Rao X, et al. Microenvironment-responsive Bletilla polysaccharide hydrogel with photothermal antibacterial and macrophage polarization-regulating properties for diabetic wound healing. *Int J Biol Macromol*. 2024;283:137819. doi:10.1016/j.ijbiomac.2024.137819
13. Ma Z, Yang X, Ma J, et al. Development of the mussel-inspired pH-responsive hydrogel based on Bletilla striata polysaccharide with enhanced adhesiveness and antioxidant properties. *Colloids Surf B*. 2021;208:112066. doi:10.1016/j.colsurfb.2021.112066
14. Zhao K, Hu Z, Chen X, et al. Bletilla striata polysaccharide-/chitosan-based self-healing hydrogel with enhanced photothermal effect for rapid healing of diabetic infected wounds via the regulation of microenvironment. *Biomacromolecules*. 2024;25(6):3345–3359. doi:10.1021/acs.biomac.4c00013
15. Nieto C, Vega MA, Enrique J, Marcelo G, Del Valle EMM. Size matters in the cytotoxicity of polydopamine nanoparticles in different types of tumors. *CANCERS*. 2019;11(11):1679. doi:10.3390/cancers11111679
16. Chen JK, Lv LY, Li Y, et al. Preparation and evaluation of *Bletilla striata* polysaccharide/graphene oxide composite hemostatic sponge. *Int J Biol. Macromol*. 2019;130:827–835. doi:10.1016/j.ijbiomac.2019.02.137
17. Li WP, Su CH, Wang SJ, et al. CO_2 delivery to accelerate incisional wound healing following single irradiation of near-infrared lamp on the coordinated colloids. *ACS NANO*. 2017;11(6):5826–5835. doi:10.1021/acsnano.7b01442
18. Li Y, Ma ZH, Yang X, et al. Investigation into the physical properties, antioxidant and antibacterial activity of Bletilla striata polysaccharide/chitosan membranes. *Int J Biol Macromol*. 2021;182:311–320. doi:10.1016/j.ijbiomac.2021.04.037
19. Huang Y, Wang P, Zhao PY, et al. ROS/Thermo dual-sensitive hydrogel loaded with a nanoemulsion of patchouli essential oil for ulcerative colitis. *Int J Biol Macromol*. 2024;281:136542.
20. Xie LM, Shen MY, Wang ZJ, Xie JH. Structure, function and food applications of carboxymethylated polysaccharides: a comprehensive review. *Trends Food Sci Technol*. 2021;118:539–557. doi:10.1016/j.tifs.2021.09.016
21. Zhang XY, Liang YP, Huang SF, Guo BL. Chitosan-based self-healing hydrogel dressing for wound healing. *Adv Colloid Interface Sci*. 2024;332 :103267.
22. Yan Q, Long XY, Zhang PX, Lei W, Sun DQ, Ye XY. Oxidized Bletilla rhizome polysaccharide-based aerogel with synergistic antibiosis and hemostasis for wound healing. *Carbohydr Polym*. 2022;293:119696.
23. Feng YQ, Qin S, Yang YM, et al. A functional hydrogel of dopamine-modified gelatin with photothermal properties for enhancing infected wound healing. *Colloids Surf B Biointerfaces*. 2024;241:114058.
24. Gao JB, Zhao ZJ, Wu B, Zhao YS. Photo-triggered CO2 release from mussel-inspired polymers. *Chem Eng J*. 2021;418:129382.
25. Guo P, Lei PK, Luo L, et al. Microfluidic-engineered Chinese herbal nanocomposite hydrogel microspheres for diabetic wound tissue regeneration. *J Nanobiotechnol*. 2024;22(1). doi:10.1186/s12951-024-02998-0
26. Fu ZZ, Zou JW, Zhong J, et al. Curcumin-loaded nanocomposite hydrogel dressings for promoting infected wound healing and tissue regeneration. *Int J Nanomed*. 2024;19:10479–10496. doi:10.2147/IJN.S479330
27. Yang H, Lv DM, Qu SQ, et al. A ROS-Responsive lipid nanoparticles release multifunctional hydrogel based on microenvironment regulation promotes infected diabetic wound healing. *Adv Sci*. 2024;11(43). doi:10.1002/advs.202403219
28. Huang XF, Shi LH, Lin Y, et al. *Pycnoporus sanguineus* polysaccharides as reducing agents: self-assembled Composite nanoparticles for integrative diabetic wound therapy. *Int J Nanomed*. 2023;18:6021–6035. doi:10.2147/IJN.S427055
29. Yang X, Jia MQ, Li Z, et al. In-situ synthesis silver nanoparticles in chitosan/Bletilla striata polysaccharide composited microneedles for infected and susceptible wound healing. *Int J Biol Macromol*. 2022;215:550–559. doi:10.1016/j.ijbiomac.2022.06.131
30. Hu ZB, Zhao K, Chen XC, et al. A berberine-loaded *Bletilla striata* polysaccharide hydrogel as a new medical dressing for diabetic wound healing. *Int J Mol Sci*. 2023;24(22):16286. doi:10.3390/ijms242216286

31. Yus C, Alejo T, Quílez C, et al. Development of a hybrid CuS-ICG polymeric photosensitive vector and its application in antibacterial photodynamic therapy. *Int J Pharm*. 2024;667:124951.
32. Zhang L, Wang KB, Zhou L, et al. Self-assembled ROS-triggered *Bletilla striata* polysaccharide-releasing hydrogel dressing for inflammation-regulation and enhanced tissue-healing. *Int J Biol Macromol*. 2024;278:135194.
33. Zhao CY, Huang L, Tang J, et al. Multifunctional nanofibrous scaffolds for enhancing full-thickness wound healing loaded with *Bletilla striata* polysaccharides. *Int J Biol Macromol*. 2024; 278:134597.
34. Cai YM, Lin PC, Li YH, et al. Alpha-ketoglutarate supramolecular network accelerates diabetic wound healing through exudates management and neovascularization. *Chem Eng J*. 2024;502 :157837.
35. Huang C, Dong LL, Zhao BH, et al. Anti-inflammatory hydrogel dressings and skin wound healing. *Clin transl med*. 2022;12(11). doi:10.1002/ctm2.1094
36. Chen C, Amona FM, Chen JH, et al. Multifunctional SEBS/AgNWs Nanocomposite films with antimicrobial, antioxidant, and anti-inflammatory properties promote infected wound healing. *ACS Appl. Mater. Interfaces*. 2024;16(45):61751–61764. doi:10.1021/acsami.4c15649
37. Shaw P, Dwivedi SKD, Bhattacharya R, Mukherjee P, Rao GT. VEGF signaling: role in angiogenesis and beyond. *BIOCHIMICA ET BIOPHYSICA ACTA-REVIEWS on CANCER*. 2024;1879(2):189079. doi:10.1016/j.bbcan.2024.189079